Appl. Phys. B 79, 77–81 (2004)
DOI: 10.1007/s00340-004-1498-2

**Applied Physics B**
**Lasers and Optics**

I. YUTSIS
B. KIRSHNER
A. ARIE✉

# Temperature-dependent dispersion relations for $RbTiOPO_4$ and $RbTiOAsO_4$

Dept. of Electrical Engineering – Physical Electronics, Faculty of Engineering, Tel-Aviv University, Tel-Aviv 69978, Israel

**Received: 25 January 2004**
**Published online: 22 April 2004 •** 

**ABSTRACT** We have measured the first and second derivatives of the refractive index with respect to temperature along the $z$- and $y$-axes for two nonlinear optical materials, $RbTiOPO_4$ and $RbTiOAsO_4$. The measurements were done using an interferometric setup in the wavelength range of 532–1580 nm and in the temperature range of 25–200 °C. In addition, the thermal expansion coefficients were measured in the $x$ direction. Experimental results of nonlinear frequency conversion in $RbTiOAsO_4$ were used to explore the temperature dependence of the refractive index in the $z$-axis near 3.5 microns. We have derived thermal-dependent dispersion equations for the two materials. Calculations based on these dispersion equations are in good agreement with previously reported measurements. The thermal dependence of the refractive index of $RbTiOAsO_4$ is greater than that of $RbTiOPO_4$ by approximately 15% and 70% in the $z$- and $y$-axes, respectively. Hence $RbTiOPO_4$ is more appropriate for applications that require immunity to thermal lensing, whereas $RbTiOAsO_4$ is suitable for realizing temperature-tuned nonlinear devices.

**PACS** 42.65.Ki, 78.20.Cy, 78.20.Nv

## 1 Introduction

Ferroelectric materials are of particular interest in nonlinear optics, owing to the possibility to achieve quasiphase matching [1] by periodic electric field poling [2].

Design and operation of temperature-tuned nonlinear optical devices, based on ferroelectric crystals, require accurate knowledge of the refractive index $n_{(\lambda,T)}$, where $\lambda$ and $T$ are the optical wavelength and temperature, respectively.

In this paper we study the thermal-dependent refractive index of two widely used nonlinear ferroelectric crystals: $RbTiOPO_4$ (RTP) and $RbTiOAsO_4$ (RTA). RTP's high electrical resistivity is important for many electro-optic applications and in the production of periodically poled RTP elements. Its high optical damage threshold makes it especially useful in high-power SHG and OPO applications [3]. RTA is an interesting material owing to its excellent transmission in the mid-infrared (IR) (up to 5.3 μm) and relatively easy poling procedure [4].

✉ Fax: +972-3/6423-508, E-mail: ady@eng.tau.ac.il

The Sellmeier equations for these two materials were given only at room temperature [4–6]. For RTA, the only available information on temperature dependence was a relative equation describing the temperature derivative of the $z$ component of the refractive index [7]. As for RTP, to the best of our knowledge, no information was available on the temperature dependence of the refractive index. Hence, it was impossible to analyze or design RTA- and RTP-based devices that operate at temperatures different than room temperature.

We have used an interferometric measurement technique that was successfully used recently for determining the thermal-dependent refractive indices of $KTiOPO_4$ (KTP) and $KTiOAsO_4$ (KTA) [8]. The thermal expansion coefficients of crystals were separately measured using another interferometric setup, thus enabling us to derive the contribution of the refractive index variations. For RTA the accuracy of the equation of $dnz/dT$ was further improved in the mid-IR using frequency conversion measurements [5]. The temperature dependence of nonlinear mixers, based on the derived Sellmeier equations, is in good agreement with previously measured values.

The experimental setup is described in Sect. 2, experimental results and analysis are given in Sect. 3, and Sect. 4 concludes and summarizes this work.

## 2 Experimental setup

The experimental setup, which is shown in Fig. 1, was built to measure the change in the optical path in the crystal as a function of the crystal temperature.

We used flux-grown RTP and RTA crystals with dimensions $10 \times 10 \times 0.5\,mm^3$. Their input and output end faces were polished perpendicular to the $x$-axis. The RTP crystal was manufactured by Raicol Crystals and the RTA crystal by Crystal Associates. Commercial lasers were exploited as coherent light sources at different wavelengths: 532 nm (frequency doubled Nd:YAG laser), 775 nm and 785 nm (external cavity diode laser), 1064 nm (Nd:YAG laser), 1520–1580 nm (external cavity diode laser). A wavemeter measured the wavelength with accuracy of 1 pm. For the measurements in the wavelength range of 1520–1580 nm the light polarization was determined with a fiber-optic polarization controller and a polarizer, and for the other wavelengths it was determined by a half-wave plate.

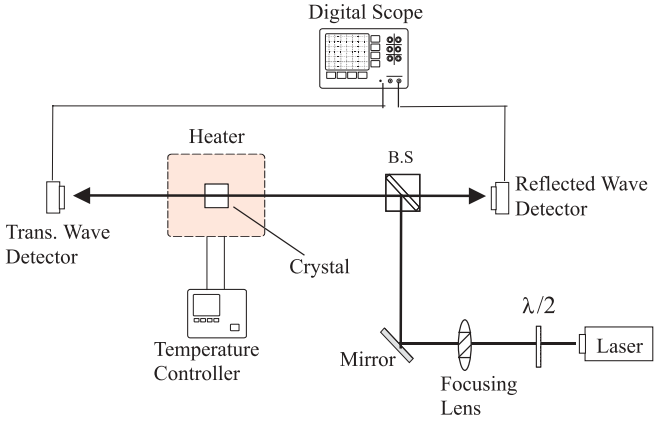


**FIGURE 1** Experimental setup for measuring the changed optical path as a function of crystal temperature

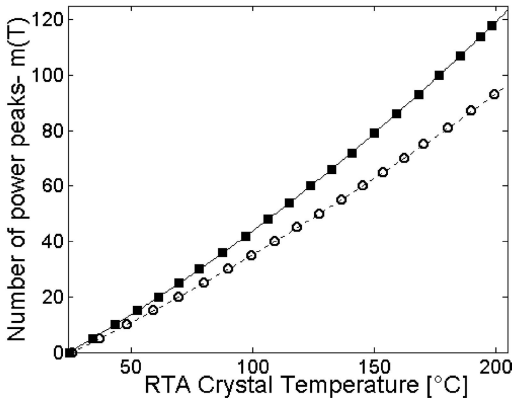


**FIGURE 2** Typical measurement of number of power peaks vs. RTA crystal temperature. The measurement was performed at wavelength $\lambda = 1549.93$ nm. Experimental results with light polarization along the $z$-axis (*squares*) and along the $y$-axis (*circles*); the *solid line* and *dotted lines* are least-square fitting curves

In order to maximize the light energy input into the crystal, a focusing lens ($f = 20$ cm) insured a beam waist of 150 μm on the crystal center. The crystal was located inside a temperature-controlled mount. This mount was comprised of a copper block, containing two heaters and a temperature sensor inside, and encompassed by a thermal insulator made of Teflon. Heaters were connected to the temperature controller, which operates in the range of 25–200 °C and with accuracy of 0.1 °C.

Light reflected from the crystal arrived at either a Si detector (for measurements below 1000 nm) or a InGaAs detector. The detector was connected to a scope, which displayed power variations as a function of crystal temperature.

The uncoated input and output facets of the measured crystal partially reflected the light. The crystal was aligned to reflect these beams in the same direction, thus leading to multiple interference, as in a Fabry–Perot cavity (1). The transmitted and reflected intensities varied periodically due to the change in optical path ($n \times l$) inside the crystal along the $x$-axis. The resonance condition for this cavity is given by

$$n_{(\lambda,T)} \times l_{(T)} = \frac{\lambda}{2} \times m_{(T)}, \tag{1}$$

where $m_{(T)}$ is the number of power peaks in the reflected light. A typical measurement in RTA with light polarized in the $y$- and $z$-axes is displayed in Fig. 2.

From (1) it is clear that it is necessary to know at high accuracy the temperature dependence of the crystal length ($l_{(T)}$ along the $x$-axis) for the derivation of the refractive index.

To measure this dependence, the crystal end faces were chemically coated with silver coating, so that the reflection was increased up to 95%. Two Michelson interferometers were established. Each one measured the expansion of one crystal end face. The experimental setup is shown in Fig. 3.

The output of a He−Ne laser (632.8 nm) contained two beams with perpendicular linear polarization and small (2 MHz) frequency difference. The polarizing beam splitter (PBS) separated the beams. One beam was directed toward the electronic unit, while the other beam propagated to the heater through a quarter-wave plate, which caused the beam to become circularly polarized. Next, the coated crystal reflected the beam. After repassing the quarter-wave plate the circular polarization reverted back to linear, though perpendicular to the original, polarization. Finally, the beam passed through the PBS to the detector.

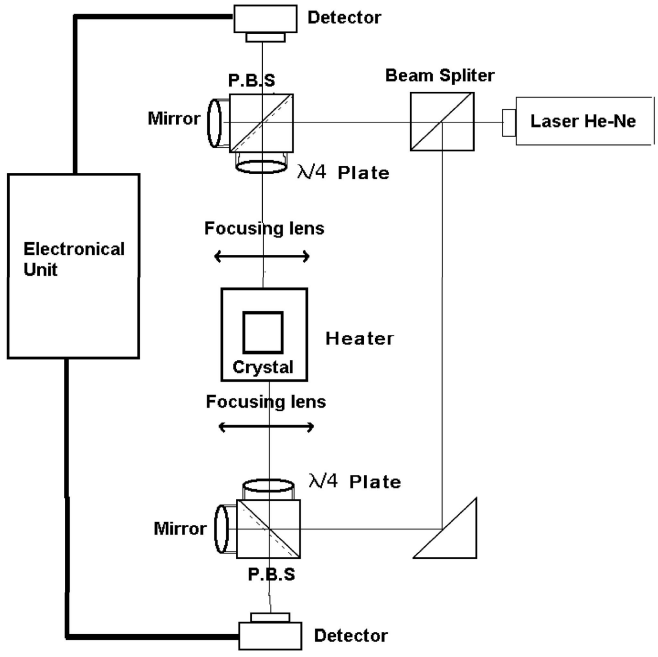


**FIGURE 3** Experimental setup for measuring thermal expansion along $x$-axis of the crystal

The electronic unit, which was very sensitive to relative phase differences between the incoming waves, translated repeated phase shifts ($\lambda/16 \sim 40$ nm) to pulses. A counter and a scope were used to summarize the optical path modifications resulting from the expansion of the heated crystal.

The contribution of the heated air around the crystal to the changed optical path was limited to 5% according to [9].

## 3 Experimental results and analysis

Equation (2) shows the dependence of the crystal length on temperature. The coefficients in the $x$-axis are depicted in Table 1. The values of the linear thermal expansion coefficient ($\alpha_x$) for the two materials were previously reported in [10]. The relative differences at a temperature of 100 °C be-

| | RTP | RTA |
|---|---|---|
| $\alpha\,[°C^{-1}]$ | $1.2733\times10^{-5}$ | $1.4468\times10^{-5}$ |
| $\beta\,[°C^{-2}]$ | $1.0285\times10^{-8}$ | $1.0454\times10^{-8}$ |

**TABLE 1** First and second thermal expansion coefficients along $x$-axis for RTP and RTA

tween our findings and values from [10] were much less than the measurement error, which is 5%:

$$l_{(T)} = l_{0(25°)} \times \left[1 + \alpha \times (T - 25°) + \beta \times (T - 25°)^2\right]. \quad (2)$$

The crystal length was determined at room temperature using the Sellmeier equations of RTA and RTP [5, 6]. $l_{0(25°)\mathrm{RTA}} = 10.695$ mm, $l_{0(25°)\mathrm{RTP}} = 9.895$ mm.

Thermal expansion coefficients and measurements of modified optical path were used to derive the refractive index change as a function of temperature:

$$n_{(\lambda,T)} = n_{0(\lambda,25°)} + n_{1(\lambda,25°)} \times (T - 25°) + n_{2(\lambda,25°)} \times (T - 25°)^2. \quad (3)$$

The first and second derivatives from (3) are presented as a third-order polynomial of negative powers of wavelength:

$$n_{1,2(\lambda,25°)} = \sum_{m=0}^{3} \frac{a_m}{\lambda^m}, \quad (4)$$

where $\lambda$ is in microns. The coefficients ($a_m$) were derived by a least-square fitting procedure and are given in Table 2.

First and second derivatives of the refractive index in RTA and RTP crystals along the $y$-axis are depicted in Figs. 4 and 5, respectively.

In order to extend our curve of $n_{1(\lambda,25°)}$ in RTA along the $z$-axis (Fig. 6) into the mid-IR range, we used measurements in quasiphase-matched difference frequency generation as a function of the crystal temperature [5]. Peak efficiency was found at a temperature of 49 °C and 64 °C with idler wavelength of 3456.1 nm and 3436.1 nm respectively, using pump wavelength of 1064.4 nm and grating period of 39.6 μm. For each temperature the corresponding wavelengths were in-

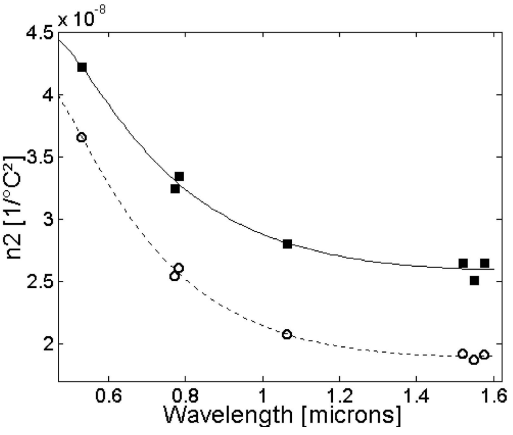


**FIGURE 5** Second derivative of the refractive index with respect to temperature versus wavelength of RTA (*squares*) and RTP (*circles*) crystals along the $y$-axis. The *solid* and the *dotted lines* are least-square fitting curves of RTA and RTP, respectively

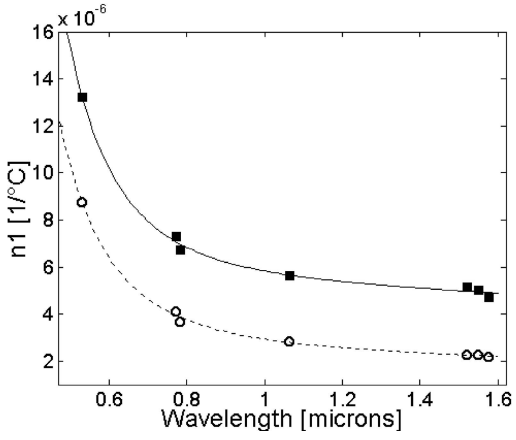


**FIGURE 4** First derivative of the refractive index with respect to temperature vs. wavelength of RTA (*squares*) and RTP (*circles*) crystals along the $y$-axis. The *solid* and *dotted lines* are least-square fitting curves of RTA and RTP, respectively

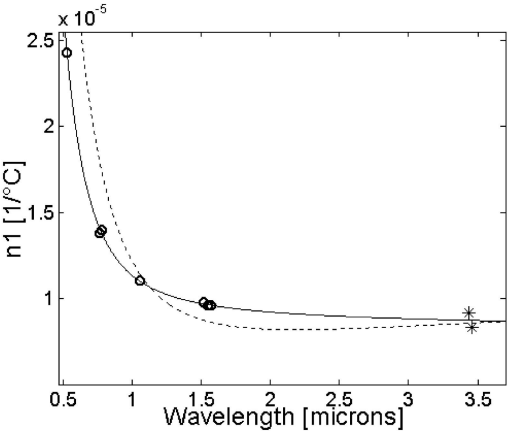


**FIGURE 6** First derivative of RTA along the $z$-axis as a function of wavelength. Experimental values (*circles*); values obtained from [5] using Eqs. 3 and 4 (*asterisks*); the *solid line* is the new and extended curve; the *dotted line* is the curve taken from [7] with the added constant (= 11 [1/°C])

| | **RTP** | | | | **RTA** | | | |
|---|---|---|---|---|---|---|---|---|
| | $z$-axis | | $y$-axis | | $z$-axis | | $y$-axis | |
| | $n_1\times10^{-6}\,[°C^{-1}]$ | $n_2\times10^{-8}\,[°C^{-2}]$ | $n_1\times10^{-6}\,[°C^{-1}]$ | $n_2\times10^{-8}\,[°C^{-2}]$ | $n_1\times10^{-6}\,[°C^{-1}]$ | $n_2\times10^{-8}\,[°C^{-2}]$ | $n_1\times10^{-6}\,[°C^{-1}]$ | $n_2\times10^{-8}\,[°C^{-2}]$ |
| $a_0$ | 13.465 | −0.858 | 0.1528 | 2.933 | 8.022 | 6.511 | 1.894 | 3.410 |
| $a_1$ | −18.336 | 14.837 | 5.712 | −3.587 | 2.936 | −6.118 | 8.548 | −3.082 |
| $a_2$ | 18.025 | −13.628 | −5.570 | 3.577 | −2.586 | 8.083 | −8.336 | 3.323 |
| $a_3$ | −3.507 | 4.4383 | 2.639 | −0.778 | 2.996 | −2.664 | 3.723 | −0.774 |

**TABLE 2** Polynomial coefficients [according to (4)] for first and second derivatives of the refractive index with respect to temperature of RTP and RTA crystals

serted into the momentum conservation equation:

$$\frac{2\pi}{\Lambda_{(T)}} - 2\pi\left(\frac{n_{(\lambda_P,T)}}{\lambda_P} - \frac{n_{(\lambda_S,T)}}{\lambda_S} - \frac{n_{0(\lambda_I,25^\circ)}}{\lambda_I} - \frac{n_{1(\lambda_I,25^\circ)}\times(T-25^\circ)}{\lambda_I} - \frac{n_{2(\lambda_I,25^\circ)}\times(T-25^\circ)^2}{\lambda_I}\right) = \Delta k. \quad (5)$$

where $n_{(\lambda_P,T)}$ and $n_{(\lambda_S,T)}$ are temperature-dependent refractive indices for the pump and the signal wavelengths ($\lambda_P$, $\lambda_S$) calculated using (3) and (4). The length of the grating period ($\Lambda_{(T)}$) for each temperature was calculated using (2). The wave vector mismatch ($\Delta k \approx 570\,\mathrm{m}^{-1}$) and $n_{0(\lambda_I,25^\circ)}$ were known from [5].

In order to extract the first derivative for the idler wavelength, we assumed the second derivative ($n_2$) was zero. This assumption can be justified since these measurements were done relatively close to room temperature, where the contribution of the second derivative is negligible. The resulting values are $n_{1(3436.1\ \mathrm{nm},25^\circ)} = 0.91\times10^{-5}\,[^\circ\mathrm{C}^{-1}]$ and $n_{1(3456.1\ \mathrm{nm},25^\circ)} = 0.83\times10^{-5}\,[^\circ\mathrm{C}^{-1}]$. Then, we added the derived values to the previously measured data of $n_1$ at shorter wavelengths and obtained a new formula for $n_{1(\lambda,T)}$, shown in (4) and Table 2. Calculation of temperature full width at half maximum of a mid-IR difference frequency generator deviated by less than 10% from measured data [5], and this further supports our assumption.

In order to compare our curve with the equation of $\mathrm{d}nz/\mathrm{d}T$ from [7], we added a constant (= 11 $[^\circ\mathrm{C}^{-1}]$) to their formula since it was derived from relative results.

Figure 6 shows the extended curve of $n_{1(\lambda,25^\circ)}$ in RTA $z$-axis and a comparison with the first derivative from [7] with the added constant.

Investigation of second harmonic generation (SHG) in PP-RTP with 1064 nm pump wavelength along the $z$-axis as a function of crystal temperature is described in [11]. Figure 7 shows good correlation between measured results of effective phase-matched grating periods taken from [11] and the calculated curve using our dispersion equations (3) and (4).

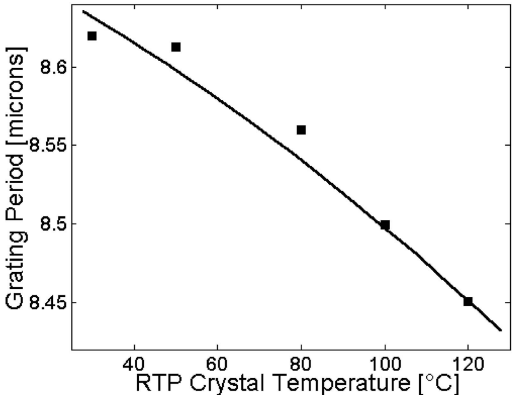


**FIGURE 7** Phase-matched grating periods as a function of RTP crystal temperature in SHG along $z$-axis with pump wavelength, $\lambda = 1064$ nm. Experimental values taken from [11] (*squares*); the *solid line* was calculated using the dispersion relation [(3) and (4)]

The inaccuracy in determining the length expansion is the dominant error in the measurements, and leads to a 5% inaccuracy in determining the thermal dependence of the refractive index.

## 4 Conclusions

We have explored the thermal dependence of the dispersion relations in RTA and RTP crystals. The temperature-dependent Sellmeier equations for these two materials are obtained in a wide temperature range (25–200 °C) and wavelength range (0.5–1.58 μm). We have experimentally observed parabolic dependence of the refractive index change on temperature. These equations are essential for insuring optimum frequency conversion efficiency in nonlinear interactions at temperatures other than room temperature as well as for designing temperature-tuned nonlinear devices. In addition, thermal expansion coefficients in the $x$-axis of the two crystals were measured with high accuracy. In QPM frequency conversion, based on periodically poled RTA or RTP, the light is usually polarized along the $z$-axis and the beam propagates along the $x$-axis. Hence, the thermal dependence of the dispersion on the $z$-axis and the thermal expansion coefficient on the $x$-axis, which have been derived in this work, are the required parameters to calculate the thermal dependence of nonlinear frequency mixers. Phase-matching calculations, based on our work, are in good agreement with previously reported measurements of temperature-dependent QPM frequency conversion with both crystals.

We have found that the thermal dependence of the refractive index of RTA is stronger than that of RTP. A comparison with results in KTP and KTA obtained from [8] shows that the thermal dependence of the refractive index of RTP is the smallest, followed by RTA, KTP, and KTA. Table 3 shows the change in refractive index from 25 °C to 100 °C at a lasing wavelength of Nd:YAG, 1064 nm for these four crystals. On the one hand, a higher refractive index thermal derivative is helpful in realizing temperature-tuned nonlinear devices; on the other hand, when high pump power is used, thermal lensing may limit the device performance [12], and in this case a low refractive index thermal derivative is an advantage. A figure of merit is proportional to the thermal conductivity and inversely proportional to the derivative of the refractive index with respect to temperature and to the material absorption coefficient [12]. The thermal conductivity of KTA, KTP, and RTA are 18 mW/cm/K [13], 30 mW/cm/K [12], and 16 mW/cm/K [14], respectively. The thermal conductivity of RTP is unknown to us. Assuming the same level of absorption can be obtained for all materials, the figure of merit for

| | $z$-axis | $y$-axis |
|---|---|---|
| RTP | $9\times10^{-4}$ (1) | $3\times10^{-4}$ (1) |
| RTA | $11\times10^{-4}$ (1.2) | $6\times10^{-4}$ (1.8) |
| KTP | $13\times10^{-4}$ (1.3) | $7\times10^{-4}$ (2.0) |
| KTA | $16\times10^{-4}$ (1.7) | $11\times10^{-4}$ (3.3) |

**TABLE 3** Change in refractive index ($\Delta n$) from 25 °C to 100 °C at wavelength $\lambda = 1064$ nm. Normalized change with respect to RTP is in parenthesis. The values are for crystals RTP, RTA, KTP, KTA. Values on KTA, KTP were taken from [9]

KTP is almost twice as high as that of KTA and RTA. RTP is also a potentially promising material for high-power applications owing to the low value of the derivative of refractive index with respect to temperature.

*Note added in Proof*: Recently, another thermo-optic dispersion equation for RTA was proposed by Kato et al [15].

**ACKNOWLEDGEMENTS** We would like to thank Shai Emanueli, Dr. Haim Feldman, and Michael Yutsis for helpful discussions.

## REFERENCES

1 J.A. Amstrong, N. Bloembergen, J. Ducuing, P.S. Pershan: Phys. Rev. **127**, 1918 (1962)
2 M. Yamada, N. Nada, M. Sitoh, K. Watanade: Appl. Phys. Lett. **62**, 435 (1993)
3 Y.S. Oseledchik, A.I. Pisarevsky, A.L. Prosvirnin, V.V. Starshenko, N.V. Svitanko: Opt. Mater. **3**, 237 (1994)
4 D.L. Fenimore, K.L. Schepler, D. Zelmon, S. Kuck, U.B. Ramabadran, P. von Richter, D. Small: J. Opt. Soc. Am. B **13**, 1935 (1996)
5 K. Fradkin-Kashi, A. Arie, P. Urenski, G. Rosenman: Appl. Phys. B **71**, 251 (2000)
6 L.K. Cheng, L.T. Cheng, J. Galperin, P.A. Morris Hotsenpiller, J.D. Bierlein: J. Cryst. Growth **137,** 107 (1994)
7 M. Peltz, U. Bader, A. Borsutzky, R. Wallenstein, J. Hellstrom, H. Karlsson, V. Pasiskevicius, F. Laurell: Appl. Phys. B **73**, 663 (2001)
8 S. Emanueli, A. Arie: Appl. Opt. **42**, 6661 (2003)
9 R. Penndorf: J. Opt. Soc. Am. **47**, 176 (1957)
10 D.K.T. Chu, J.D. Bierlein, R.G. Hunsperger: Trans. Ultrason. **39**, 683 (1992)
11 I. Juwiler: PhD dissertation, Tel-Aviv University (2003)
12 I. Juwiler, A. Arie: Appl. Opt. **42**, 7163 (2003)
13 http://www.cristal-laser.fr/Pages/products/KTA/data.htm
14 http://www.cristal-laser.fr/Pages/products/RTA/data.htm
15 K. Kato, E. Takaoka, N. Umemura: Jpn. J. Appl. Phys **42**, 6420 (2003)